A Concept for an Interferometric SAR Mission with Sub-daily Revisit

Jalal Matar[a], Maria J. Sanjuan-Ferrer[a], Marc Rodriguez-Cassola[a], Susan Steele-Dunne[b], and Francesco De Zan[c]
[a]Microwaves and Radar Institute, German Aerospace Center (DLR), 82334 Weßling, Germany
[b]Faculty of Civil Engineering and Geosciences, Delft University of Technology, 2628 CN Delft, The Netherlands
[c]delta phi remote sensing GmbH, 82205 Gilching, Germany

Abstract

This paper introduces a SAR mission concept uniquely designed for sub-daily interferometric-compatible revisits, essential for the timely monitoring of ecosystem water status in regions of significant scientific, ecological, societal, and economic value. The key concept is based on the strategic deployment of a constellation of several small satellites in short-revisit low-Earth orbits, equipped with low complexity SAR payloads to enhance efficiency and minimize overall costs. In particular, L-band SARs with decametric spatial resolution and sub-daily revisit will be considered. The paper provides an overview of the mission requirements, technical concept, scientific relevance, and acquisition potential. The analysis is based on a study conducted in the frame of an ESA Earth Explorer 12 mission proposal titled "SLAINTE" [1].

1 Introduction

As climate variability intensifies and anthropogenic pressures on land and water resources escalate, the imperative for ecosystem monitoring has never been more pronounced. The ability to track sub-daily variations in vital parameters, such as surface soil moisture and vegetation water content across target regions, is paramount to understanding the adaptability and resilience of terrestrial ecosystems and their associated water resources [2]. These observations are essential to address ESA's Living Planet Challenges in atmospheric, land, and solid Earth domains [3].

The introduction of an L-band interferometric SAR mission with sub-daily revisits offers a pivotal advancement in Earth observation. This mission's data will complement that from contemporary passive and active sensors, such as SMAP, SMOS, ASCAT, ERS, among others. Crucially, it aims to fill a fundamental gap in our current spatial-temporal observation capabilities [1].

The proposed mission concept features a constellation of identical SAR satellites, each operating in a short-revisit low Earth orbit (LEO). The strategic positioning of these monostatic satellites allows for sub-daily data acquisitions with a 6-hour lag from successive satellite passes - for instance, at 6 am, 12 pm and 6 pm. While the preliminary concept incorporates three satellites, offering observational access to more than $39\,\%$ of the land mass, there is potential for expansion to accommodate additional lags or broader observational access. The L-band SAR payload has been carefully designed to meet stringent mass and cost constraints. Consequently, this has led to the integration of a highly efficient, low-power system paired with a 5-meter deployable reflector antenna.

2 Orbit Characteristics

In this section we provide a succinct overview of the orbit selection and insertion strategy for the proposed mission concept.

2.1 Orbit Selection

To meet requirements such as frequent revisits, simplified radar payload design, reduced power consumption, and access to at least $25\,\%$ of the terrestrial surface, a sun-synchronous orbit (SSO) at lower LEO altitudes emerged as the optimal choice for the orbit selection.

Given the mission's monostatic operation and simplified payloads, orbital configurations with three-day repeat cycles strike an effective balance between revisit frequency and access area. Specifically, they enable coverage of over $25\,\%$ of the Equator, with a combined swath width ranging from 200 to $220\,\mathrm{km}$. Consequently, we selected a 3/46 SSO at $460\text{-}\mathrm{km}$ altitude, providing access to $39\,\%$ of the global land mass from either ascending or descending passes, with an incident angle range of $30°$ to $48.28°$. Fig.

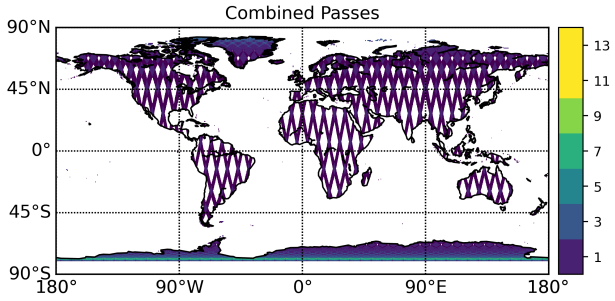

Figure 1 Potential land access from a three-day repeat sun-synchronous orbit at $460\text{-}\mathrm{km}$ altitude in right-looking geometry. The plotted area corresponds to an incident angle range of $30°$ to $48.28°$.

Table 1 Orbital elements of the three satellites of the suggested constellation.

Orbit parameter	Sat A	Sat B	Sat C
Semi-major axis [km]		6837.975	
Inclination [°]		97.25	
Eccentricity		0.001182612	
Argument of perigee [°]		90	
RAAN [°]	Ω_0	Ω_0-90	Ω_0-180

1 illustrates the access area from combined passes, accumulating to 59 % of the global landmass. This choice also requires moderate budgets for orbit maintenance, approximately 15 m/sec delta-V per year for the initial spacecraft design.

Table 1 presents the orbital elements of the selected orbits for each satellite. The reference right ascension of the ascending node (RAAN), denoted as Ω_0, serves as a design parameter which can be tuned to enhance coverage and revisit times over specific areas of interest, e.g., in Europe, the Sahel or the Amazonia. As indicated, each satellite in the constellation operates in a unique orbital plane. These planes are offset by 90° in RAAN, effectively utilizing Earth's rotation to achieve the desired 6-hour intervals between successive satellite passes while maintaining consistent observation geometries.

2.2 Insertion Strategy

Preliminary assessments of the spacecraft, considering the incorporation of a 5-meter deployable reflector antenna, indicate that each satellite conforms to the small-satellite class specifications, i.e., weighing under 500 kg. As per the logistical capacities of the Vega-C launcher [4], a dual-launch configuration can accommodate a maximum of two such satellites, with volume serving as the primary constraint. Therefore, two separate Vega-C launches would be necessary: one dual launch for satellites A and B and a subsequent single launch for satellite C into the 460-km orbit. As mentioned earlier, the existing design permits potential expansion to a four-satellite constellation, entailing dual-launch configurations for both launches. Fig. 2 (left) provides a graphical representation of the satellites in their operational orbit.

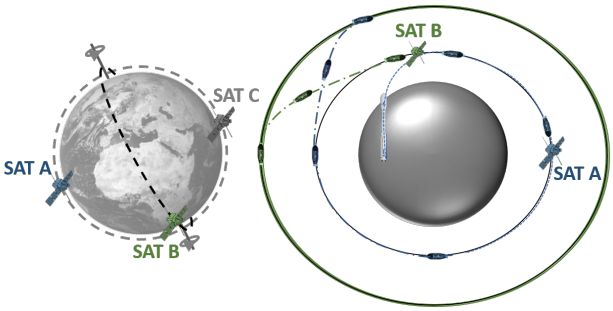

Figure 2 (left) Representation of the concept constellation in orbit. (right) Graphical representation of the strategy followed to achieve the 90-degree shift in RAAN.

For the dual-launch case, a direct insertion of the two spacecraft into distinct orbital planes with a 90-degree shift in RAAN would be prohibitively expensive in terms of fuel. Hence, we have devised an insertion tactic which has minor impact on the complexity of the spacecraft yet extends the insertion duration for one of the satellites. Fig. 2 (right) illustrates this process in which the first spacecraft is released into the reference 460-km orbit, while the second one is brought to an altitude of 1046 km. According to Vega-C specifications [4], the launcher can lift approximately 2400 kg to 460 km and around 1800 kg to 1046 km, providing a comfortable margin for this process. Once flying at different altitudes, the higher satellite's reduced drift results in a 90-degree RAAN divergence within a year. The prevailing strategy involves retaining the second spacecraft without immediate release. This approach allows the launch capsule to drift over the span of a year, after which we execute an orbital transfer (e.g., Hohmann) utilizing the launcher's propulsion system to transition the satellite to its final orbit at 460 km, where it is released. Based on our numbers, the cost of the orbit transfer is a delta-V of around 307 m/sec, which would be allocated as part of the launcher.

3 Instrument Characteristics

In line with our strategy to engineer a lightweight solution for a SAR system operating in L-band, we opted for a large deployable reflector (LDR) antenna with a 5-meter diameter. We specifically chose a stripmap imaging mode and a low operational altitude (e.g., 460 km), to optimize the overall efficiency in terms of Watts per pixel [5, 6]. Based on these characteristics, the desired access area, and the relevant backscattering laws from Ulaby, we derived the system parameters and performance figures, which are comprehensively presented in Table 2.

As shown, the radar is designed to comply with five different rolls, covering an access area of around 218 km. This configuration allows the mission to image up to 39 % of the land mass in either ascending or descending passes. Note that the excursion of the NESN (and SNR) has a variation of 6 dB (to better values). Additionally, the PRF has been tailored to ensure the absence of gaps from transmit events and nadir returns. The integration of a resolution spanning 500 m^2 and a sensitivity approximating −20 dB ensures commendable radiometric sensitivity for the L1 products. Better resolutions can be accommodated for interferometric products derived from the three sub-daily interferograms. Fig 3 shows a simulated interferogram assuming the imaging characteristics of the proposed mission. The results were generated using a DLR End-to-End (E2E) simulator [7]. Notice the pronounced clarity of the fringes in the interferogram, generated for a product resolution of 100 m × 100 m and considering thermal decorrelation only. Fig. 4 shows a sample reflectivity image that we can potentially get using the system parameters described in Table 2.

Table 2 Main system and imaging performance parameters for the radar instrument.

Parameter	Roll 1	Roll 2	Roll3	Roll4	Roll5
LDR Diameter [m]			5		
Peak power [W]			390		
Average power [W]			50		
Residual roll pointing [°]	0.07	0.07	0.07	-0.04	0.07
SLC resolution [m^2]			500 (e.g., 5.34 x 93.64)		
Swath overlap [km]			1		
Swath width [km]	39.6	40	48.77	43.72	49.71
Near incidence [°]	30	33.86	37.47	41.5	44.8
Far incidence [°]	33.95	37.56	41.6	44.87	48.28
PRF [Hz]	3486	3665	3222	3558	2916
Bandwidth [MHz]	3.2	2.87	2.63	2.41	2.27
SNR [dB]	> 7.6	> 7.8	> 4.33	> 5.9	> 5
NESN [dB]	< -22.6	< -23.7	< -21	< -24	< -23.6
ASR (AASR, RASR) [dB]	<-29 (-29, -31)	<-26 (-32, -27)	<-22 (-22, -26)	<-21 (-30, -21)	<-17 (-17, -19)
Radiometric resolution [dB]	<0.1 @1 km^2 resolution				

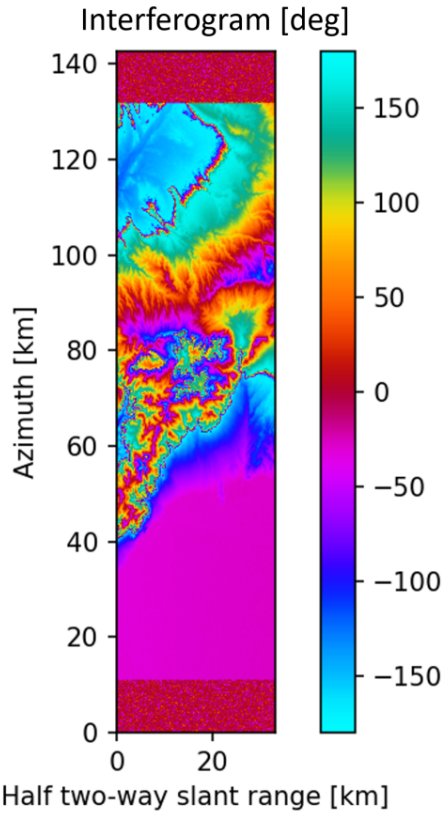

Figure 3 Sample interferogram generated using the DLR E2E simulator [7]. The simulation corresponds to a product resolution of 100 m × 100 m and considering ideal conditions (i.e., only considering thermal decorrelation).

4 Acquisition Strategy Potential

The formulation of an initial acquisition strategy is shaped by considerations such as the available system resources, accessibility constraints, and the scientific objectives of the mission, specifically the desired mission products.

Despite the use of compact platforms for the suggested SAR systems, their monostatic operation and high efficiency are expected to allow extended operational duration, e.g., 20 minutes per orbit for both SAT A and SAT C (depicted in Fig. 2 left). For SAT B, which encounters repetitive eclipse fractions close to 50 % (e.g., in the descending pass), the operational window is anticipated to be around 12 minutes.

In terms of accessibility, the system can perform 5 rotations within an incident angle range of 30° to 48.28°, allowing access to 59 % of the global landmass. This capability is achieved while meeting the performance metrics outlined in Table 2. With a unique pass orientation, e.g., ascending, access to 39 % of the land mass is possible, maintaining the 6-hour lag from acquisitions at 6 am, 12 pm, and 6 pm. Conversely, the other orientation, e.g., descending, provides access to an additional 39 % of the landmass, with acquisitions at 6 pm, 12 am, and 6 am. Although global coverage is not part of the planned mission scope, it remains feasible by drifting the orbital planes over different mission phases, thereby achieving a cumulative swath of around 870 km.

Each roll provides coverage of 7 % to 9 % of the landmass, in a single orientation, across any of the 39 % accessible area with a three-day revisit interval. Table 3 compares potential global landmass coverage using ascending, descending (LC asc/desc) or combined passes (LC combined), across four example acquisition strategies: (AS1) acquiring all scenes with a three-day revisit, (AS2) acquiring 75 % of the scenes with a three-day revisit and 25 % with a twelve-day revisit, (AS3) acquiring 50 % of the scenes with a three-day revisit, 16.7 % with a six-day revisit, 16.7 % with a nine-day revisit, and 16.7 % with a twelve-day revisit, and (AS4) acquiring 25 % of

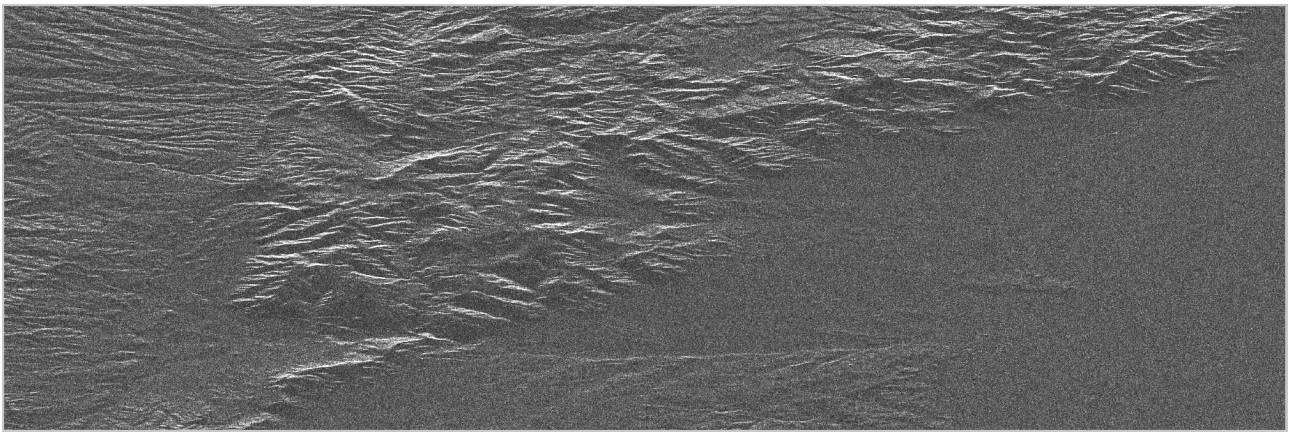

Figure 4 Reflectivity image provided by the DLR E2E simulator for the end-to-end simulation of the suggested instrument under ideal conditions.

Table 3 Comparison of example acquisition strategies: distribution of revisit intervals (three-, six-, nine-, and twelve-day revisit) and their corresponding global landmass cover (LC) percentage.

	AS1	**AS2**	**AS3**	**AS4**
three-day	100 %	75 %	50 %	25 %
six-day	0 %	0 %	16.7 %	25 %
nine-day	0 %	0 %	16.7 %	25 %
twelve-day	0 %	25 %	16.7 %	25 %
LC asc/desc	7 %	12.8 %	14.7 %	18.4 %
LC combined	13.4 %	22.2 %	25.5 %	31.5 %

scenes with three-, six-, nine-, and twelve-day revisit intervals each. These acquisition strategies may be employed throughout the mission or during the initial phase to evaluate the variability of acquired data across different revisit times, thereby facilitating dynamic selection of revisit times to optimize mission objectives and coverage.

In terms of mission objectives, the primary regions of interest, highlighted by the red rectangles in Fig. 5, encompass most of Europe, Amazonia, and parts of Sahel. These regions are considered crucial for the mission's identified products and overarching objectives. The covered swaths in the plot are conservative and correspond to AS1. The maximum acquisition time per orbit required to cover the longest ascending-pass swath is 8 minutes, well within the satellite's resources. This underscores that the available system resources permit the coverage of additional regions through semi-independent passes, and further regions with independent passes, e.g., over Asia and North America. A good example of semi-independent passes is Greenland, which in combination with the three other polygons would result in a maximum acquisition time per orbit of 10.6 minutes. Fig. 6 shows the coverage over Greenland from (top) ascending and (bottom) descending using the first four rolls, while ensuring a twelve-day revisit interval. This information can hold significance when compared with data acquisitions anticipated from the forthcoming ROSE-L ESA mission. A more detailed acquisition plan will be developed in future phases of the mission.

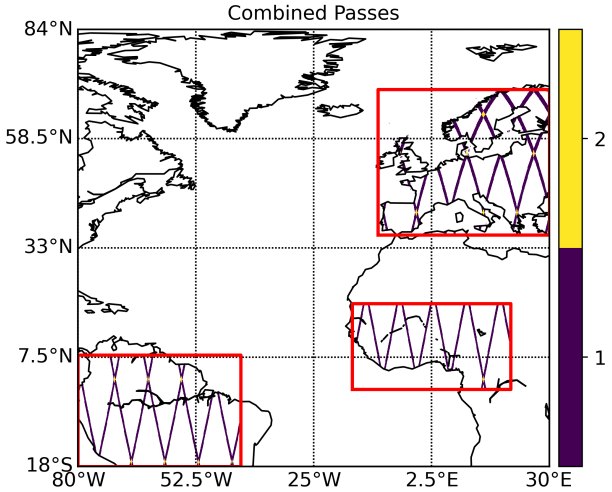

Figure 5 Capturing 5.5 % of the land mass in targeted regions across Europe, Amazonia, and Sahel during either ascending or descending passes. The cumulative coverage from combined passes extends to 10.5 %.

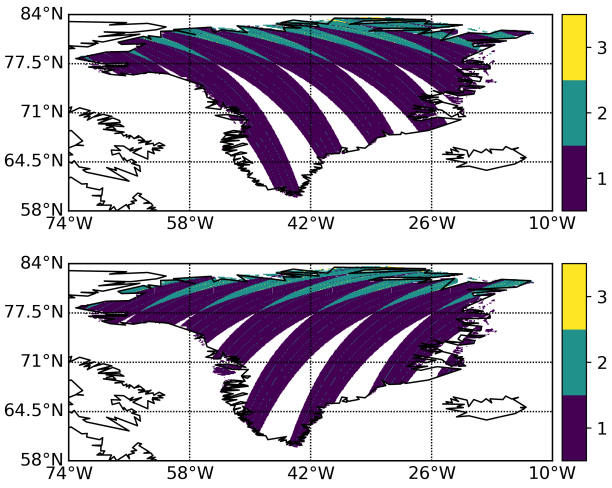

Figure 6 Potential Greenland coverage with a twelve-Day revisit interval and four rolls from (top) ascending and (bottom) descending satellite passes. Each pass orientation covers 74 % of the landmass, totaling 89.4 % if combined.

5 Mission Elements

In this section we report briefly on the main mission objectives and products to be achieved and delivered with the proposed mission.

5.1 Mission Objectives

The mission aims to address observation gaps in ecosystem water status by tracking sub-daily variations in vital parameters such as soil moisture and vegetation water content. These parameters are crucial for estimating sub-daily terrestrial evaporation, understanding the coupling mechanisms between carbon and water cycles, quantifying sub-daily stress response of vegetation, and monitoring vegetation health. Additionally, they will facilitate quantifying agricultural water use, explaining processes that drive the triggering and evolution of flash floods and landslides, and understanding the influence of vegetation and soil water status on convective storm predictability [1].

5.2 Mission Products

The L-band radar backscatter data will be used to retrieve surface soil moisture, vegetation water content, plant water potential, and wet/dry canopy state with a 1-km^2 resolution.

Given the interferometric sensitivity of SAR phase to both soil and vegetation [8], the interferometric data can be used to extract surface soil moisture and vegetation water content values with better resolutions, as illustrated in the interferogram in Fig 3. Despite the complexity of direct extraction, numerous studies have demonstrated a link between soil moisture and closure phase [9, 10, 11]. The closure phase represents the circular combination of multi-looked interferograms, obtained from three or more acquisition periods, remains free from undesirable contributions, notably atmospheric conditions. In theory, inverting multiple closure phases allows the generation of a chronologically ordered series of soil moisture variations or vegetation water content variations sampled according to the original revisit time [10, 11, 12].

6 Outlook

This paper introduces the technical concept for an L-band interferometric SAR mission, featuring sub-daily revisit capability and compelling interferometric and radiometric performance. The proposed mission employs a constellation of three compact SAR satellites, ensuring three consecutive passes over designated regions of interest with a 6-hour interval. Remarkably, the design achieves compliance with small-class platforms, even at a longer wavelength, through careful optimization of system, orbit and launch parameters, emphasizing light-weight solutions.

7 References

[1] S. Steele-Dunne, A. Bastos, F. de Zan, W. Dorigo, S. Lhermitte, C. Massari, J. Matar, D. Milodowski, D. Miralles, A. Monteith, M. Rodriguez Cassola, C. Taylor, S. Tebaldini, and Ulander L. SLAINTE: A SAR mission concept for sub-daily microwave remote sensing of vegetation. In *EUSAR 2024; 15th European Conference on Synthetic Aperture Radar*, pages 1–3, 2024.

[2] M. Scholze, M. Buchwitz, W. Dorigo, L. Guanter, and S. Quegan. Reviews and syntheses: Systematic Earth observations for use in terrestrial carbon cycle data assimilation systems. *Biogeosciences*, 14(14):3401–3429, 2017.

[3] A. O'Neill, D. Barber, P. Bauer, H. Dahlin, M. Diament, D. Hauglustaine, PY. Le Traon, F. Mattia, W. Mauser, C. Merchant, et al. Earth Observation Science Strategy for ESA: A New Era for Scientific Advances and Societal Benefits. *Earth Observation Science Strategy*, 2015.

[4] R. Lagier. Ariane 5 User's Manual. Technical report, Arianespace, 2018. Issue 0, Revision 0.

[5] M. Rodriguez Cassola, J. Matar, N. Sakar, and E. Rodrigues-Silva. Distributed SAR for Space 4.0: Performance Models and E2E Definition. Technical report, DLR, 2022. Doc. No. DistSAR4.0-DLR-DI-1. ESA Contract No. EOP-ΦMM/2018-01-2060/NG/ng.

[6] J. Matar, M. Rodriguez Cassola, E. Rodrigues-Silva, N. Sakar, V. Gracheva, M. Suess, G. Krieger, and A. Moreira. A LEO-SAR Constellation Equivalent to an Interferometric Geosynchronous Mission. In *IEEE International Geoscience and Remote Sensing Symposium (IGARSS)*, 2023.

[7] M. Rodriguez-Cassola, P. Prats, M. Pinheiro, M. Zonno, M. Nannini, M. Sanjuan-Ferrer, N. Yague-Martinez, F. Bordoni, T. Boerner, G. Krieger, and A. Moreira. End-to-end Level-0 Data Simulation Tool for Future Spaceborne SAR Missions. In *EUSAR 2018; 12th European Conference on Synthetic Aperture Radar*, pages 1–6, 2018.

[8] K. Morrison, J. C. Bennett, M. Nolan, and R. Menon. Laboratory Measurement of the DInSAR Response to Spatiotemporal Variations in Soil Moisture. *IEEE Transactions on Geoscience and Remote Sensing*, 49(10):3815–3823, 2011.

[9] F. De Zan, A. Parizzi, and P. Prats-Iraola, P.and López-Dekker. A SAR Interferometric Model for Soil Moisture. *IEEE Transactions on Geoscience and Remote Sensing*, 52 (1):418–425, 2014. doi: 10.1109/TGRS.2013.2241069.

[10] F. De Zan, M. Zonno, and P. López-Dekker. Phase Inconsistencies and Multiple Scattering in SAR Interferometry. *IEEE Transactions on Geoscience and Remote Sensing*, 53 (12):6608–6616, 2015. doi: 10.1109/TGRS.2015.2444431.

[11] S. Zwieback, S. Hensley, and I. Hajnsek. Soil Moisture Estimation Using Differential Radar Interferometry: Toward Separating Soil Moisture and Displacements. *IEEE Transactions on Geoscience and Remote Sensing*, 55(9):5069–5083, 2017. doi: 10.1109/TGRS.2017.2702099.

[12] F. De Zan and G. Gomba. Vegetation and soil moisture inversion from SAR closure phases: First experiments and results. *Remote sensing of environment*, 217:562–572, 2018.

[13] S. Zwieback, S. Hensley, and I. Hajnsek. Assessment of soil moisture effects on L-band radar interferometry. *Remote Sensing of Environment*, 164:77–89, 2015.